3-D Diffusive Molecular Communication with Two Fully-Absorbing Receivers: Hitting Probability and Performance Analysis

Nithin V. Sabu, Neeraj Varshney and Abhishek K. Gupta

Abstract

Exact analytical channel models for molecular communication via diffusion (MCvD) systems involving multiple fully absorbing receivers (FARs) in a three-dimensional (3-D) medium are hard to obtain due to the mathematical intractability of corresponding diffusion equations. Therefore, this work considers an MCvD system with two spherical FARs in a 3-D diffusion-limited medium and develop several insights using an approximate analytical expression for the hitting probability of information molecule (IM). Further, based on the hitting probability, a novel approximate closed-form analytical expression for the area under the receiver operating characteristic curve (AUC) is derived to analyze the detection performance at each FAR in the presence of other FAR. Finally, simulation results are presented to validate the analytical results using the particle-based and Monte-Carlo simulations and to yield important insights into the MCvD system performance with two FARs.

I. Introduction

In recent times, the Internet of Bio-Nano Things (IoBNT) is gaining significant prominence towards addressing challenging problems in biomedical scenarios, where multiple transmitters and receivers have to work together to perform complex tasks, including sensing and actuation [1]. In this context, molecular communication via diffusion (MCvD) has gained significant research attention to realize communication between bio-nano-machines within the IoBNT. In an MCvD system, information molecules (IMs) emitted from the transmitter propagates to the receiver via Brownian motion [2].

N. V. Sabu and A. K. Gupta are with Indian Institute of Technology Kanpur, Kanpur UP 208016, India (Email: {nithinvs,gkrabhi}@iitk.ac.in). N. Varshney is with the Wireless Networks Division, National Institute of Standards and Technology, Gaithersburg, MD 20899 USA (Email: neerajv@ieee.org).

Related Work: In the context of multiple devices communicating using MCvD, [3] considers an MCvD system with two FARs in a 3D medium and obtains the hitting probability of an IM at each fully-absorbing receiver (FAR), or equivalently the average fraction of IMs absorbed by each FAR. Note that in contrast to passive receiver where the receiver does not affect the propagation of IMs, a FAR immediately absorbs the IMs once they hit its surface [2]. The channel model derived in [3] consists of two unknowns, which have to be computed numerically. To the best of our knowledge, the exact expressions of the hitting probability for systems with multiple FARs are not available in the literature. Due to the lack of analytical channel model for an MCvD system with multiple FARs in 3D medium, most of the works [4]–[6] relied on simulation-based channel models to analyze the system performance. In the past, [7] studied the 3D kinetics of a Brownian particle in the presence of two spherical traps and presented an approximate expression for the death probability of this particle from any of these two traps. This analytical framework can be applied to derive channel models for MCvD systems with two FARs and study its performance, which is the prime focus of this letter. The derived channel model has applications in a variety of interesting scenarios, including (1) interference and performance analysis of an MCvD system with two FARs (since transmitters as well as absorbing receivers can cause interference in the communication) and (2) MIMO systems with two FARs that act as receiving units to a common receiver.

Contributions: In this letter, we consider an MCvD system with one transmitter and two spherical FARs in a diffusion-limited 3D medium and develop a channel model based on the analysis in [7]. Using the proposed channel model, we further develop an analytical framework to study such systems. We then validate the presented analysis via particle-based simulations. We provide several design insights related to the mutual influence of FARs and their mutual distance's impact on the hitting probability of an IM on each FAR. We also derive the area under the receiver operating characteristic curve (AUC) for each individual FAR, which serves as a quantitative measure for the FAR's capability of correct decision and study the impact of the presence of another FAR on it. We also provide a novel approximate closed-form analytical expression for AUC.

II. SYSTEM MODEL

In this letter, we consider an MCvD system with a point transmitter and two spherical FARs at different locations in a 3D medium as shown in Fig. 1. Let the transmitter be located at the
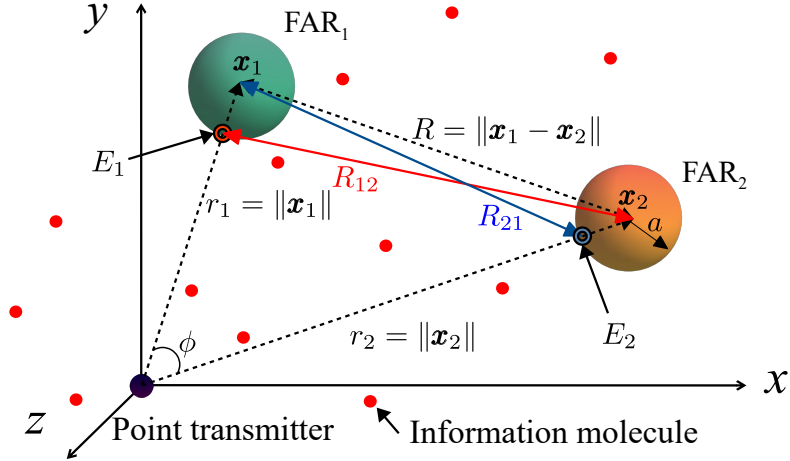
Fig. 1: A 3D MCvD system with a point transmitter at the origin and two FARs located at $\boldsymbol{x}_1$ and $\boldsymbol{x}_2$. E_i denotes the closest point of ith FAR from the transmitter.

origin and the two FARs of radius a at positions $\boldsymbol{x}_1$ and $\boldsymbol{x}_2$ respectively in $\mathbb{R}^3$ space. The time is divided into time-slots of duration T_S, *i.e.* lth time-slot denotes the time period $[(lT_\mathrm{S}, (l+1)T_\mathrm{S}]$ with $l \geq 0$. At the beginning of each time-slot, the transmitter transmits its binary information using the on-off keying modulation, *i.e.* the transmitter emits N IMs for bit 1 and does not emit any IMs for bit 0. IMs have a diffusion coefficient D with respect to the propagation medium. We assume D to be constant over the space and time. In any time-slot l, the transmit bit $b[l]$ is an independent Bernoulli random variable taking value 1 with probability q_1, and 0 with $q_0 = 1 - q_1$. The transmitter and both FARs are assumed to be synchronized in time, which is a common assumption in the past literature [6].

The probability that an IM reaches (and gets absorbed by) the ith FAR located at $\boldsymbol{x}_i$ within time t in the presence of the other FAR located at $\boldsymbol{x}_j$, is denoted by $\mathrm{p}(t, a, r_i, r_j)$. Here $r_i = \|\boldsymbol{x}_i\|$ and $r_j = \|\boldsymbol{x}_j\|$. This *hitting probability* equals the average fraction of IMs absorbed until time t by the ith FAR. Let us now focus on a particular time-slot l. Now, the probability that an IM emitted at the kth slot reaches in the lth slot at ith FAR can be written in terms of $\mathrm{p}(t, a, r_i, r_j)$ as

$$h_i[l-k] = \mathrm{p}((l-k+1)T_\mathrm{S}, a, r_i, r_j) - \mathrm{p}((l-k)T_\mathrm{S}, a, r_i, r_j), \tag{1}$$

$\forall l \geq k$. In particular, $h_i[0]$ denotes the probability that IM transmitted in lth time-slot arrives in the same time-slot. We assume that there are no potential collisions between the IMs during their propagation in the medium [2], and hence, the motion of an IM is independent of the motion

of other IMs. Thus, $S_i[l]$ denoting the number of IMs reaching the FAR_i in the lth time-slot corresponding to bit $b[l]$ is Binomial distributed with parameters $Nb[l]$ and $h_i[0]$, *i.e.* $S_i[l] \sim \mathcal{B}(Nb[l], h_i[0])$. Note that if n is large, $\mathcal{B}(n, q)$ can be approximated as Gaussian distribution $\mathcal{N}(\mu, \sigma^2)$ with mean $\mu = nq$ and variance $\sigma^2 = nq(1 - q)$ [2]. Hence, we can model $S_i[l] \sim \mathcal{N}(Nb[l]h_i[0], Nb[l]h_i[0](1 - h_i[0]))$. Similarly, $I_i[k]$ denoting the number of IMs received at the FAR_i in lth time-slot corresponding to the transmission in kth slot $(k < l)$ can be modeled as

$$I_i[k] \sim \mathcal{N}\left(Nb[k]h_i[l-k], Nb[k]h_i[l-k](1 - h_i[l-k])\right).$$

Note that, $I_i[k]$ corresponds to inter symbol interference (ISI) arising due to the transmission from previous kth time-slot. Now, the total number of IMs corresponding to all previous transmissions is $I_i[l] = \sum_{k=1}^{l-1} I_i[k]$. Let $N_i[l]$ denote the number of molecules received from unintended sources with $N_i[l] \sim \mathcal{N}(\mu_\text{n}, \sigma_\text{n}^2)$ [8]. Now, $Y_i[l]$ denoting the total number of molecules arriving at FAR_i in the lth time-slot, is given as

$$Y_i[l] = S_i[l] + I_i[l] + N_i[l]. \tag{2}$$

During detection, FAR_i decodes $\widehat{b}_i[l] = 1$ when $Y_i[l] \geq \eta_i$ and $\widehat{b}_i[l] = 0$ otherwise, where η_i is the decision threshold. Before proceeding further, we will calculate the mean $\mu_{b[l]}[i; l]$ and variance $\sigma_{b[l]}^2[i; l]$ of the random variable $Y_i[l]$ for $b[l] \in \{0, 1\}$, which would be useful when analyzing the performance of the receiver in Section IV. These can be derived as

$$\mu_0[i; l] = Nq_1 \sum_{k=1}^{l-1} h_i[l-k] + \mu_\text{n},$$

$$\sigma_0^2[i; l] = Nq_1 \sum_{k=1}^{l-1} \left[h_i[l-k](1 - h_i[l-k]) + Nq_0 h_i[l-k]^2 \right] + \sigma_\text{n}^2,$$

$$\mu_1[i; l] = Nh_i[0] + \mu_0[i; l],$$

$$\sigma_1^2[i; l] = Nh_i[0](1 - h_i[0]) + \sigma_0^2[i; l].$$

In contrast to Genie-aided approach where the means and the variances are obtained in terms of previous bits [9], we assume the previous bits to be random and take average over them for the above calculations [10]. In the next section, we will discuss the hitting probability $\text{p}(t, a, r_i, r_j)$ for each of the FARs and their influence on each other.

III. Mutual Influence of the Two FARs

The exact analytical expression for $p(t, a, r_i, r_j)$ in a 3D medium is not available in the existing literature due to its intractability. However, using the analytical framework given in [7], an approximate value for it can be obtained as,

$$p(t, a, r_i, r_j) = \sum_{n=0}^{\infty} \frac{a^{2n}}{R_{ij}^n R_{ji}^n} \left[\frac{a}{r_i} \text{erfc} \left(\frac{r_i - a + n(R_{ji} - a) + n(R_{ij} - a)}{\sqrt{4Dt}} \right) \right.$$
$$\left. - \frac{a^2}{r_j R_{ji}} \text{erfc} \left(\frac{r_j - a + (n+1)(R_{ji} - a) + n(R_{ij} - a)}{\sqrt{4Dt}} \right) \right], \tag{3}$$

where R_{ji} is the distance between the center of ith FAR and the closest point of jth FAR from the origin (E_j, see Fig. 1). If ϕ is the angle between vectors $\boldsymbol{x}_1$ and $\boldsymbol{x}_2$, then $R_{ji} = \sqrt{(r_j - a)^2 + r_i^2 - 2(r_j - a) \cdot r_i \cos(\phi)}$. The approximation is good under the assumptions- (i) the distance between the transmitter and each FAR is significantly larger than a, *i.e.* $r_1 \gg a$ and $r_2 \gg a$, and (ii) the distance between FAR$_1$ and the FAR$_2$ is significantly larger than a, *i.e.* $R = \|\boldsymbol{x}_i - \boldsymbol{x}_j\| \gg a$. Note that $\text{erfc}(z) = \frac{2}{\sqrt{\pi}} \int_z^{\infty} \exp(-t^2) dt$ is the complementary error function. The proof of (3) is included in Appendix A. Further note that, the fraction of IMs absorbed within time t by the FAR$_i$ (denoted by $\overline{p}(t, a, r_i)$) in the absence of any other FAR is [11]

$$\overline{p}(t, a, r_i) = \frac{a}{r_i} \text{erfc} \left(\frac{r_i - a}{\sqrt{4Dt}} \right). \tag{4}$$

From (3) and (4), we can develop several important insights that are presented below.

Corollary 1. *The fraction of IMs eventually hitting FAR$_i$ in the absence and the presence of FAR$_j$ are*

$$\overline{p}(\infty, a, r_i) = \frac{a}{r_i}, \text{ and } p(\infty, a, r_i, r_j) = \frac{a R_{ij}}{R_{ij} R_{ji} - a^2} \left[\frac{R_{ji}}{r_i} - \frac{a}{r_j} \right]. \tag{5}$$

Therefore, the presence of FAR$_j$ reduces the eventual hitting probability at FAR$_i$ by the amount

$$s_i(\infty, a) = \overline{p}(\infty, a, r_i) - p(\infty, a, r_i, r_j) = \frac{a^2}{R_{ij} R_{ji} - a^2} \left[\frac{R_{ij}}{r_j} - \frac{a}{r_i} \right], \tag{6}$$

which denotes the fraction of IMs that would have hit FAR$_i$ eventually, but instead hit FAR$_j$ first and got absorbed.
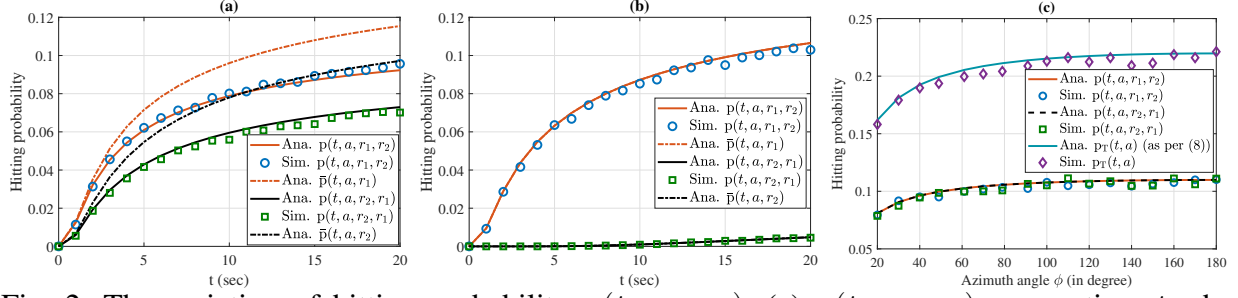
Fig. 2: The variation of hitting probability $p(t, a, r_i, r_j)$. (a) $p(t, a, r_i, r_j)$ versus time t when $\boldsymbol{x}_1 = [30, 0, 0]$ and $\boldsymbol{x}_2 = [30, 15, 0]$. (b) $p(t, a, r_i, r_j)$ versus t when $\boldsymbol{x}_1 = [-30, -10, 0]$ and $\boldsymbol{x}_2 = [100, 40, 0]$. (c) $p(t, a, r_i, r_j)$ versus the angular distance ϕ between the two FARs at time $t = 15$s. The minimum azimuth angle is taken as 20° to avoid the overlap of FARs. The solid/dashed lines represent the analytical expression (terms $< 10^{-16}$ are neglected), and markers represent the values obtained via particle-based simulations. Here, analytical values of $p(t, a, r_i, r_j)$ and $\overline{p}(t, a, r_i)$ are as per (3) and (4) respectively.

Corollary 2. *When the two FARs are far apart, (i.e. $R \to \infty$. Note that, $R \to \infty \implies R_{ij}, R_{ji} \to \infty$),*

$$p(t, a, r_i, r_j) \to \frac{a}{r_i}\mathrm{erfc}\left(\frac{r_i - a}{\sqrt{4Dt}}\right) = \overline{p}(t, a, r_i). \tag{7}$$

In other words, the mutual influence of FARs vanishes as they move away from each other.

Corollary 3. *The probability that an IM reaches any of the FARs is*

$$p_T(t, a) = p(t, a, r_1, r_2) + p(t, a, r_2, r_1). \tag{8}$$

A. Validation

We first validate the expression (3) of $p(t, a, r_i, r_j)$ through particle-based simulations which are carried out for 10^4 iterations, with a step size of 10^{-4} s. D is 100 μm/s^2, and both FARs have radius $a = 5 \mu$m, which are the same for all numerical evaluations in this paper unless stated otherwise. Fig. 2 (a) and (b) show the hitting probability of IM on each of the FARs in presence of the other for two different cases. Fig. 2 (a) shows the variation of hitting probability with t when $\boldsymbol{x}_1 = [30, 0, 0]$ and $\boldsymbol{x}_2 = [30, 15, 0]$ and Fig. 2 (b) shows the variation of hitting probability with t when $\boldsymbol{x}_1 = [-30, -10, 0]$ and $\boldsymbol{x}_2 = [100, 40, 0]$. In the Fig. 2 (a), the FARs are relatively closer to each other with $R = 15$ μm. In Fig. 2 (b), the two FARs are relatively far away with $R = 139.2$ μm. We can observe that the analytical expression (3) closely matches with

simulation results for both cases. We can also observe that in Fig. 2 (a), FARs have a significant influence on each other, which grows with time t as seen by the widening gap between solid and dashed lines. In Fig. 2 (b), the distance between FARs is large enough, resulting in a negligible mutual influence. Also, the hitting probability of the FAR closer to the transmitter of the two FARs is higher than that of the other one.

From extensive numerical simulations, we found that the absolute error (|analytical approximate value − exact value|) of the hitting probability expression for each FAR is negligible when $r_1>3a$, $r_2>3a$ and $R>3a$ implying the goodness of approximation under these conditions. Note that, the conditions r_1, $r_2>a$ and $R>2a$ is a prerequisite to avoid the overlap between FARs and FAR and transmitter.

B. Impact of Distance R on Hitting Probability

We now study the impact of mutual distance on the hitting probability of an IM on FARs equidistant from the transmitter. Without loss of generality, we consider one FAR at x-axis with $r_1=20$ μm and other FAR in x-y-plane with the same radial distance $\|\boldsymbol{x}_2\|=r_1$ and azimuth angle ϕ. Note that, the distance depends on ϕ as $R=2\|\boldsymbol{x}_2\|\sin(\phi/2)$. Fig. 2 (c) shows the variation of hitting probability with varying azimuth angular distance ϕ between the two FARs. Here also, we can observe that for the chosen parameters, the analytical and simulation results match well, including the scenario when the FARs are close to each other. Fig. 2 (c) also shows the total probability $\mathrm{p_T}(t,a)$. It can be verified that $\mathrm{p_T}(t,a) = 2\mathrm{p}(t,a,r_1,r_2)$. This is because the fraction of IMs absorbed by each FARs are the same owing to their equal distance from the transmitter.

C. Comparison of two FARs vs single FAR

We now study the gain $g(t,a)$ that can be achieved by replacing one FAR by two FARs at two different locations. In particular, in the first scenario, there is only one FAR of radius a at $\boldsymbol{x}_1$ with hitting probability of IM as $\overline{\mathrm{p}}(t,a,r_1)$. Now, in the second scenario, there are two FARs, each of radius b at two different locations $\boldsymbol{x}_1$ and $\boldsymbol{x}_2$ such that $r_1 = r_2$. For a fair comparison, we keep the total surface area of the FARs equal in both scenarios *i.e.* $b=a/\sqrt{2}$. The hitting probability of an IM on any of the FARs is $\mathrm{p_T}(t,a/\sqrt{2})=2\mathrm{p}(t,a/\sqrt{2},r_1,r_2)$. We can see that for any time t,

$$g(t,a) = \frac{\mathrm{p_T}(t,a/\sqrt{2})}{\overline{\mathrm{p}}(t,a,r_1)} < \frac{\sqrt{2}\mathrm{erfc}\left(\frac{r_1-a/\sqrt{2}}{\sqrt{4Dt}}\right)}{\mathrm{erfc}\left(\frac{r_1-a}{\sqrt{4Dt}}\right)} < \sqrt{2} \tag{9}$$

which upper bounds the gain. Further, using the following lower and upper bounds [12] of erfc:

$$\frac{e^{-x^2}}{\sqrt{\pi}x}\left(1 - \frac{1}{2x^2}\right) < \text{erfc}(x) < \frac{e^{-x^2}}{\sqrt{\pi}x}$$

in the denominator and numerator terms of $g(t,a)$, we can show that, for any t,

$$g(t,a) < \frac{r_1 - a}{r_1 - \frac{a}{\sqrt{2}}}\frac{\exp\left(-\frac{(2-\sqrt{2})ar_1 - a^2/2}{4Dt}\right)}{\left(\frac{1}{\sqrt{2}} - \frac{\sqrt{2}Dt}{(r_1-a)^2}\right)}, \tag{10}$$

which is less than 1 for small t. This implies that for small t, the scenario with a single FAR gives better hitting probability.

However, when $t \to \infty$ and $R_{ij} > a(1 + 1/\sqrt{2})$, (5) gives

$$g(\infty, a) = \frac{\text{p}_\text{T}(\infty, a/\sqrt{2})}{\overline{\text{p}}(\infty, a, r_1)} = \frac{2R_{ij}}{\sqrt{2}R_{ij} + a} > 1, \tag{11}$$

which implies that the hitting probability of an IM on any of the FARs of radius $a/\sqrt{2}$ is higher than the scenario with a single FAR of radius a. Fig. 3 compares the two scenarios. It can be seen that initially, the single FAR gives better hitting probability. This is due to the close proximity of the surface of a single FAR of radius a than two FARs of radius $a/\sqrt{2}$ to the transmitter. However, as time t increases, the total hitting probability of IM on any one of the two FARs becomes larger, which is consistent with the above analysis. This increase in hitting probability is due to the absorption of IM in more directions by the two FAR case compared to that of a single FAR case.

IV. DETECTION PERFORMANCE AT FARS

Let $\text{P}_{\text{d},i}(\eta_i, l)$ and $\text{P}_{\text{f},i}(\eta_i, l)$ denote the detection and false alarm probabilities at FAR_i in the lth time-slot, respectively. Applying the binary hypothesis testing [13] on $Y_i[l]$ for the detection of bit $b[l]$, $\text{P}_{\text{d},i}(\eta_i, l)$ and $\text{P}_{\text{f},i}(\eta_i, l)$ can be derived from (2) as

$$\text{P}_{\text{d},i}(\eta_i, l) = \mathbb{P}\left[Y_i[l] > \eta_i \mid b[l] = 1\right] = Q\left(\frac{\eta_i - \mu_1[i; l]}{\sigma_1[i; l]}\right), \tag{12}$$

$$\text{P}_{\text{f},i}(\eta_i, l) = \mathbb{P}\left[Y_i[l] > \eta_i \mid b[l] = 0\right] = Q\left(\frac{\eta_i - \mu_0[i; l]}{\sigma_0[i; l]}\right). \tag{13}$$

Here, $Q(x) = 0.5\text{erfc}\left(x/\sqrt{2}\right)$ is the standard Q-function.

The receiver operating characteristic (ROC) curve illustrates the variation of the detection probability with respect to the false alarm probability for a receiver by varying detection threshold as an intermediate variable. The area under the ROC curve (AUC) is a quantitative measure of a
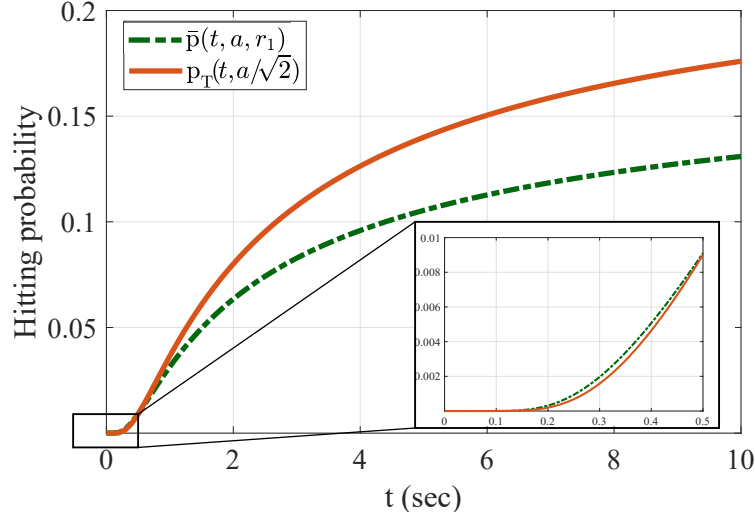
Fig. 3: Comparison of the hitting probability of IMs for the case with a single FAR of radius a located at $\boldsymbol{x}_1 = [25\ 0\ 0]$ vs the case with two receivers of radius $a/\sqrt{2}$ at $\boldsymbol{x}_1 = [25\ 0\ 0]$ and $\boldsymbol{x}_2 = [-25\ 0\ 0]$. Here, $a = 5\mu m$.

receiver's capability of correct decision [14]. The AUC value can vary from 0 to 1, where AUC = 0 indicates that bits are always erroneously decoded, and AUC = 1 indicates the perfect decoding without any error. Moreover, AUC = 0.5 indicates that the receiver is unable to distinguish between 0 and 1. The AUC for the FAR_i in lth time-slot is [14]

$$A_i[l] = \int_0^1 P_{d,i}(\eta_i, l) dP_{f,i}(\eta_i, l). \tag{14}$$

$$= \frac{1}{\sqrt{2\pi}\sigma_0[i;l]} \int_0^\infty Q\left(\frac{\eta_i - \mu_1[i;l]}{\sigma_1[i;l]}\right) \times \exp\left(-\frac{(\eta_i - \mu_0[i;l])^2}{2\sigma_0^2[i;l]}\right) d\eta_i. \tag{15}$$

Applying approximation on Q-function, a closed-form approximation for AUC at FAR_i in lth time-slot is derived as

$$A_i[l] \approx \frac{1}{2\sqrt{2}\sigma_0[i;l]} \sum_{\kappa=1}^3 \frac{(-1)^{\kappa+1}}{\sqrt{a_\kappa}} \exp\left(\frac{b_\kappa^2 - a_\kappa c_\kappa}{a_\kappa}\right)$$

$$\times \left[\text{erfc}\left(e_\kappa + \frac{b_\kappa}{\sqrt{a_\kappa}}\right) - \text{erfc}\left(\frac{\sqrt{a_\kappa}}{d_\kappa \mu_1[i;l]} + \frac{b_\kappa}{d_\kappa \sqrt{a_\kappa}}\right)\right], \tag{16}$$

where $\alpha=0.3842$, $\beta=0.7640$, $\gamma=0.6964$, $a_1 = 0.5\sigma_0^{-2}$, $b_1 = -\mu_0 a_1$, $c_1 = \mu_0^2 a_1$, $d_1 = 1$, $e_1 = 0$, $a_2 = \alpha\sigma_1^{-2} + a_1$, $b_2 = -(\alpha\mu_1 + \beta\sigma_1/2)\sigma_1^{-2} + b_1$, $c_2 = (\alpha\mu_1 + \beta\sigma_1)\mu_1\sigma_1^{-2} + c_1 + \gamma$, $d_2 = 1$, $e_2 = 0$, $a_3 = a_2$, $b_3 = -(\alpha\mu_1 - \beta\sigma_1/2)\sigma_1^{-2} + b_1$, $c_3 = (\alpha\mu_1 - \beta\sigma_1)\mu_1\sigma_1^{-2} + c_1 + \gamma$, $d_3 = 0$, $e_3 = \sqrt{a_3}\mu_1$ for respective i and l.

Fig. 4(a) shows the AUC variation with N for both FARs in $l=10$th slot for $T_S = 5$s. It can be observed that the AUC values at both FARs significantly improve as N increases. This

improvement in AUC is due the fact that the gap between $Y_i[l]$ for $b[l] = 1$ and $b[l] = 0$ increases with N with respect to the noise $N_i[l]$, and the variance of $S_i[l]$ does not increases relatively as much as its mean with N. Further we can observe that, the receiver closer to the transmitter, which is FAR_1 here, has larger AUC than FAR_2 which indicates better decision capability of FAR_1. We also study a scenario with two FARs working together to make a joint detection. In this case, $Y[l] = Y_1[l] + Y_2[l]$ is compared with threshold η to make a decision for bit $b[l]$. The AUC of this joint detection is given by (36) with the mean and variance values as $\mu_0[l] = \mu_0[1; l] + \mu_0[2; l]$, $\mu_1[l] = \mu_1[1; l] + \mu_1[2; l]$, $\sigma_0^2[l] = \sigma_0^2[1; l] + \sigma_0^2[2; l]$ and $\sigma_1^2[l] = \sigma_1^2[1; l] + \sigma_1^2[2; l]$ respectively. Fig. 4(a) also shows the AUC of this system. It can be seen that its AUC is higher than individual AUC of both FARs which is intuitive. An ideal implementation of such system would require a central node which is transparent to IMs for combining the observation from FARs. Hence, these AUC values serve as the upper bound to any practical implementation.

Fig. 4(b) shows variation in the AUC with distance between the two FARs. Here, $N = 1000$ and $T_S = 1$s. FAR_1 is fixed at $\boldsymbol{x}_1 = [-10, 0, 0]$. The location of the FAR_2 is $\boldsymbol{x}_2 = [-10 + R, 0, 0]$ which is moved in positive x-direction by increasing R. It can be seen that the increment in R results in higher distance between transmitter and FAR_2, which in turn deteriorates the detection capability at FAR_2. It is interesting to note that even though influence of FAR_1 on FAR_2 reduces with increase in R, the gain in the number of received IMs at FAR_2 is superseded by the loss of IMs due to increase in distance of FAR_2 from the transmitter. The performance at FAR_1 improves slightly since the number of IMs reaching FAR_1 increases due to the diminishing influence of FAR_2 on FAR_1 with increase in R. One can also note that both FARs have identical AUC values when they are located at an equal distance from the transmitter.

V. CONCLUSIONS

For a 3D MCvD system with multiple FARs, there is no analytical channel model in the current literature. In this work, we have tried to bridge this gap by presenting an approximate analytical expression for hitting probability of an IM considering two FARs in $\mathbb{R}^3$ space. We have developed several important insights that are lacking in the current literature. Moreover, this work explicitly demonstrated the impact of receiver locations on their mutual dependency. We have found that the use of two distantly located receivers can increase the total hitting probability by covering two different directions of molecular movement from the transmitter compared to the use of single FAR in one direction. Using the hitting probability expression, this work analyzed
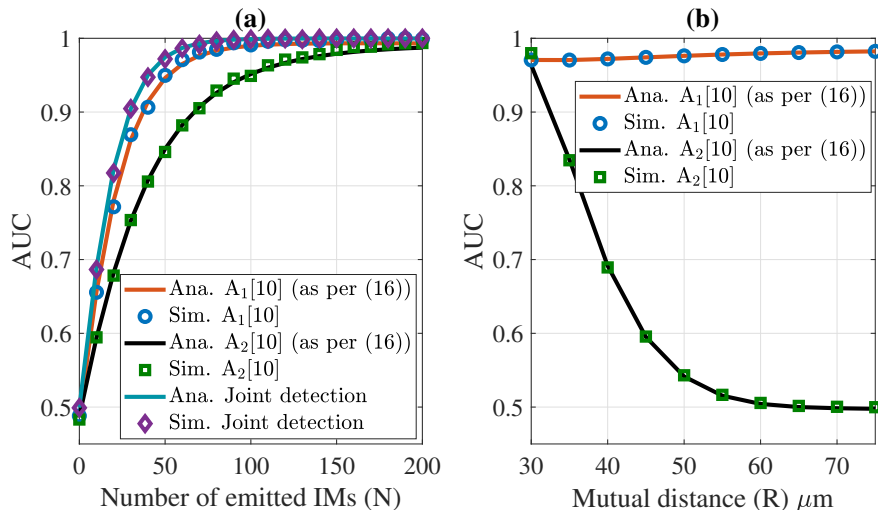
Fig. 4: (a) AUC of the individual FARs vs N (number of emitted IMs). Here, $\boldsymbol{x}_1 = [20, 5, 0]$ and $\boldsymbol{x}_2 = [-25, -10, 0]$. (b) Impact of mutual distance R between the two FARs on their AUC. For both figures, $\mu_n = \sigma_n^2 = 5$. The solid lines represent the analytical values obtained using (16), whereas the markers represent the values obtained using Monte-Carlo simulations.

the detection performance at both FARs in terms of AUC and quantified the impact of their location on their detection capability. Future work can now focus on (a) characterizing the 3D channel for more than two FARs by applying similar techniques discussed in this work, and (b) applying presented results in the analysis of large scale networks.

APPENDIX A

DERIVATION OF (3)

The probability that an IM emitted by the point source at origin hits the surface of FAR_j in the interval $[\tau, \ \tau + \mathrm{d}\tau]$ is $\left[\frac{\mathrm{dp}(t, a, r_j, r_i)}{\mathrm{d}\tau} \right] \mathrm{d}\tau$. The probability that this IM hits the FAR_i in the remaining $t - \tau$ time is $\overline{\mathrm{p}}(t - \tau, a, d_{ji})$, where d_{ji} is the distance between the IM's hitting point at the surface of FAR_j and the center of FAR_i. Note that d_{ji} is a random variable. To simplify the analysis, we approximate the term $\overline{\mathrm{p}}(t - \tau, a, d_{ji})$ by $\overline{\mathrm{p}}(t - \tau, a, R_{ji})$, where R_{ji} is the distance between E_j (the nearest point on the surface of FAR_j from the transmitter) and the center of FAR_i (see Fig. 1). The probability of an IM that is supposed to hit the FAR_i within time t, but gets absorbed at FAR_j before hitting FAR_i is [7, Eq. 13] [15, Eq. A2]

$$\overline{\mathrm{p}}(t, a, r_i) - \mathrm{p}(t, a, r_i, r_j) = \int_0^t \frac{\partial \mathrm{p}(t, a, r_j, r_i)}{\partial \tau} \overline{\mathrm{p}}(t - \tau, a, R_{ji}) \mathrm{d}\tau. \tag{17}$$

Similarly, the probability of an IM that is supposed to hit the FAR$_j$ within time t, but is hitting the FAR$_i$ before it, is

$$\overline{\mathrm{p}}(t,a,r_j)-\mathrm{p}(t,a,r_j,r_i)=\int_0^t \frac{\partial \mathrm{p}(t,a,r_i,r_j)}{\partial \tau}\overline{\mathrm{p}}(t-\tau,a,R_{ij})\mathrm{d}\tau. \tag{18}$$

Now, taking the Laplace transform (LT) of (17) and (18) gives

$$\overline{\mathcal{P}}(s,a,r_i)-\mathcal{P}(s,a,r_i,r_j)=s\mathcal{P}(s,a,r_j,r_i)\overline{\mathcal{P}}(s,a,R_{ji}), \tag{19}$$

$$\overline{\mathcal{P}}(s,a,r_j)-\mathcal{P}(s,a,r_j,r_i)=s\mathcal{P}(s,a,r_i,r_j)\overline{\mathcal{P}}(s,a,R_{ij}), \tag{20}$$

where $\overline{\mathcal{P}}(s,a,r_i)$, $\mathcal{P}(s,a,r_i,r_j)$ and $\overline{\mathcal{P}}(s,a,R_{ij})$ are the LTs of $\overline{\mathrm{p}}(t,a,r_i)$, $\mathrm{p}(t,a,r_i,r_j)$ and $\overline{\mathrm{p}}(t,a,R_{ij})$, respectively.

Solving (19) and (20) gives

$$\mathcal{P}(s,a,r_i,r_j)=\frac{\overline{\mathcal{P}}(s,a,r_i)-s\overline{\mathcal{P}}(s,a,r_j)\overline{\mathcal{P}}(s,a,R_{ji})}{1-s^2\overline{\mathcal{P}}(s,a,R_{ij})\overline{\mathcal{P}}(s,a,R_{ji})}, \tag{21}$$

where $\overline{\mathcal{P}}(s,a,x)$ can be solved as

$$\overline{\mathcal{P}}(s,a,x)=\mathcal{L}\left[\frac{a}{x}\mathrm{erfc}\left(\frac{x-a}{\sqrt{4Dt}}\right)\right]=\frac{a}{x}\frac{\exp\left(-(x-a)\sqrt{\frac{s}{D}}\right)}{s}.$$

Finally, substituting the above expression in (21) and taking the inverse LT gives (3).

Supplementary file to '3-D Diffusive Molecular Communication with Two Fully-Absorbing Receivers: Hitting Probability and Performance Analysis'

APPENDIX B

DERIVATION OF MEAN $\mu_{b[l]}[i;l]$ AND VARIANCE $\sigma^2_{b[l]}[i;l]$ OF $Y_i[l]$

From (2), we know

$$Y_i[l] = S_i[l] + \sum_{k=1}^{l-1} I_i[k] + N_i[l] \tag{22}$$

with

$$S_i[l] \sim \mathcal{N}(Nb[l]h_i[0], Nb[l]h_i[0](1 - h_i[0]))$$

$$I_i[k] \sim \mathcal{N}(Nb[k]h_i[l-k], Nb[k]h_i[l-k](1 - h_i[l-k]))$$

$$N_i[l] \sim \mathcal{N}(\mu_{\mathrm{n}}, \sigma^2_{\mathrm{n}}).$$

Also for time-slot $k < l$, the transmit bit $b[k]$ is an independent Bernoulli random variable taking value 1 with probability q_1, and 0 with $q_0 = 1 - q_1$. Hence $\mathbb{E}[b[k]] = q_1$.

Now, given the bit transmitted at the current slot l *i.e.* $b[l]$, the mean of the random variable $Y_i[l]$ is given

$$
\begin{aligned}
\mu_{b[l]}[i;l] &= \mathbb{E}[Y_i[l]] \\
&= Nh_i[0]b[l] + \mathbb{E}\left[\sum_{k=1}^{l-1} Nb[k]h_i[l-k]\right] + \mu_{\mathrm{n}} \\
&= Nh_i[0]b[l] + Nq_1 \sum_{k=1}^{l-1} h_i[l-k] + \mu_{\mathrm{n}}.
\end{aligned}
\tag{23}
$$

For the derivation of variance of $Y_i[l]$, first, we derive the variance of $I_i[k]$. The mean of $I_i[k]$ given $b[k]$ is

$$\mathbb{E}[I_i[k] \mid b_i[k]] = Nb[k]h_i[l-k]. \tag{24}$$

The variance of $I_i[k]$ given $b[k]$ is

$$\mathrm{Var}\left(I_i[k] \mid b[k]\right) = Nb[k]h_i[l-k](1 - h_i[l-k]). \tag{25}$$

From (24) and (25), the variance of $I_i[k]$ can be derived as

$$
\begin{aligned}
\mathrm{Var}\left(I_i[k]\right) =&\mathbb{E}\left[\mathrm{Var}(I_i[k] \mid b_i[k])\right] + \mathrm{Var}(\mathbb{E}[I_i[k] \mid b_i[k]]) \\
=&Nq_1 h_i[l-k](1-h_i[l-k]) + N^2 h_i[l-k]^2 \mathrm{Var}\left(b[k]\right) \quad\quad (26) \\
=&Nq_1 h_i[l-k](1-h_i[l-k]) + N^2 h_i[l-k]^2 q_1 q_0 \quad\quad\quad\quad (27)
\end{aligned}
$$

Therefore, variance of $Y_i[l]$ given the current transmitted bit $b[l]$ is

$$
\begin{aligned}
\sigma^2_{b[l]}[i;l] =&\mathrm{Var}(S_i[l]) + \mathrm{Var}(I_i[l]) + \mathrm{Var}(N_i[l]) \\
=&Nb[l]h_i[0](1-h_i[0])+Nq_1 \sum_{k=1}^{l-1} \left[h_i[l-k](1-h_i[l-k])\right. \\
&\left.+Nq_0 h_i[l-k]^2\right] + \sigma^2_n. \quad\quad\quad\quad\quad\quad\quad\quad\quad\quad (28)
\end{aligned}
$$

APPENDIX C

DERIVATION OF (10)

Using (3) and (4), for any t,

$$
g(t,a) = \frac{\mathrm{p_T}(t,a/\sqrt{2})}{\overline{\mathrm{p}}(t,a,r_1)} < \frac{\sqrt{2}\mathrm{erfc}\left(\frac{\|\boldsymbol{x}_1\|-a/\sqrt{2}}{\sqrt{4Dt}}\right)}{\mathrm{erfc}\left(\frac{\|\boldsymbol{x}_1\|-a}{\sqrt{4Dt}}\right)}. \quad\quad\quad (29)
$$

Now, using the following upper and lower bounds [12] of erfc:

$$
\frac{e^{-x^2}}{\sqrt{\pi}x}\left(1-\tfrac{1}{2x^2}\right) < \mathrm{erfc}(x) < \frac{e^{-x^2}}{\sqrt{\pi}x},
$$

at the numerator and the denominator respectively of (29) gives

$$
\frac{\mathrm{p_T}(t,a/\sqrt{2})}{\overline{\mathrm{p}}(t,a,r_1)} < \frac{\dfrac{\sqrt{2}\exp\left(-\left(\frac{\|\boldsymbol{x}_1\|-a/\sqrt{2}}{\sqrt{4Dt}}\right)^2\right)}{\sqrt{\pi}\left(\frac{\|\boldsymbol{x}_1\|-a/\sqrt{2}}{\sqrt{4Dt}}\right)}}{\dfrac{\exp\left(-\left(\frac{\|\boldsymbol{x}_1\|-a}{\sqrt{4Dt}}\right)^2\right)}{\sqrt{\pi}\left(\frac{\|\boldsymbol{x}_1\|-a}{\sqrt{4Dt}}\right)} \times \left(1 - \dfrac{1}{2\left(\frac{\|\boldsymbol{x}_1\|-a}{\sqrt{4Dt}}\right)^2}\right)}. \quad (30)
$$

Simplifying (30) gives

$$
\frac{\mathrm{p_T}(t,a/\sqrt{2})}{\overline{\mathrm{p}}(t,a,r_1)} < \frac{\|\boldsymbol{x}_1\| - a}{\|\boldsymbol{x}_1\| - \frac{a}{\sqrt{2}}} \frac{\exp\left(-\frac{(2-\sqrt{2})a\|\boldsymbol{x}_1\|-a^2/2}{4Dt}\right)}{\left(\frac{1}{\sqrt{2}} - \frac{\sqrt{2}Dt}{(\|\boldsymbol{x}_1\|-a)^2}\right)}, \quad\quad (31)
$$

which is (10) in the submitted manuscript.

APPENDIX D

DERIVATION OF (11)

The inequality shown in (11) can be derived from (5) as

$$g(t, a) = \frac{\mathrm{p_T}(\infty, a/\sqrt{2})}{\overline{\mathrm{p}}(\infty, a, r_1)} = \frac{\frac{2 \times a/\sqrt{2}}{\|\boldsymbol{x}_1\|} \times \frac{R_{ij}}{R_{ij} + a/\sqrt{2}}}{\frac{a}{\|\boldsymbol{x}_1\|}}$$

$$= \sqrt{2} \times \frac{R_{ij}}{R_{ij} + a/\sqrt{2}}$$

$$= \frac{2R_{ij}}{\sqrt{2}R_{ij} + a} \tag{32}$$

Note that, $R > a$ for transmitter to not to overlap with the FAR and $R \gg a$ ($R \gg a \implies R_{ij} \gg a$) for (3) to be valid with minimum error. When $R_{ij} > a\left(1 + 1/\sqrt{2}\right)$, (32) is

$$g(\infty, a) = \frac{\mathrm{p_T}(\infty, a/\sqrt{2})}{\overline{\mathrm{p}}(\infty, a, r_1)} = \frac{2R_{ij}}{\sqrt{2}R_{ij} + a} > 1, \tag{33}$$

which is (11) in the submitted manuscript.

APPENDIX E

DERIVATION OF (16)

The probability of false alarm $\mathrm{P}_{\mathrm{f},i}(\eta_i, l)$ varies monotonically from 0 to 1 when η_i changes from ∞ to 0. Thus, (14) can be equivalently written as [14]

$$\mathrm{A}_i[l] = -\int_0^\infty \mathrm{P}_{\mathrm{d},i}(\eta_i, l) \frac{\mathrm{dP}_{\mathrm{f},i}(\eta_i, l)}{\mathrm{d}\eta_i} \mathrm{d}\eta_i, \tag{34}$$

where

$$\frac{\mathrm{dP}_{\mathrm{f},i}(\eta_i, l)}{\mathrm{d}\eta_i} = -\frac{1}{\sqrt{2\pi}\sigma_0[i; l]} \exp\left(-\frac{(\eta_i - \mu_0[i; l])^2}{2\sigma_0^2[i; l]}\right). \tag{35}$$

Further, substituting the above expression along with (13) in (17), the $\mathrm{A}_i[l]$ can be written as

$$\mathrm{A}_i[l] = \frac{1}{\sqrt{2\pi}\sigma_0[i; l]} \int_0^\infty Q\left(\frac{\eta_i - \mu_1[i; l]}{\sigma_1[i; l]}\right)$$

$$\times \exp\left(-\frac{(\eta_i - \mu_0[i; l])^2}{2\sigma_0^2[i; l]}\right) \mathrm{d}\eta_i. \tag{36}$$

Finally, splitting the above integral into two separate integrals with limits from 0 to $\mu_1[i; l]$ and from $\mu_1[i; l]$ to ∞, and subsequently using the following tight and more tractable approximation[1] for $Q(x)$ [16]

$$Q(x) \approx \begin{cases} \exp(-\alpha x^2 - \beta x - \gamma) & \text{if } x \geq 0 \\ 1 - \exp(-\alpha x^2 + \beta x - \gamma) & \text{if } x < 0, \end{cases} \tag{37}$$

(where $\alpha = 0.3842$, $\beta = 0.7640$ and $\gamma = 0.6964$) and then, using the following integral identity from [17, Eq. 2.33.1], *i.e.*

$$\int e^{-(ax^2 + 2bx + c)} \mathrm{d}x = \frac{1}{2}\sqrt{\frac{\pi}{a}} \exp\left(\frac{b^2 - ac}{a}\right) \mathrm{erf}\left(\sqrt{a}x + \frac{b}{\sqrt{a}}\right),$$

we get (16).
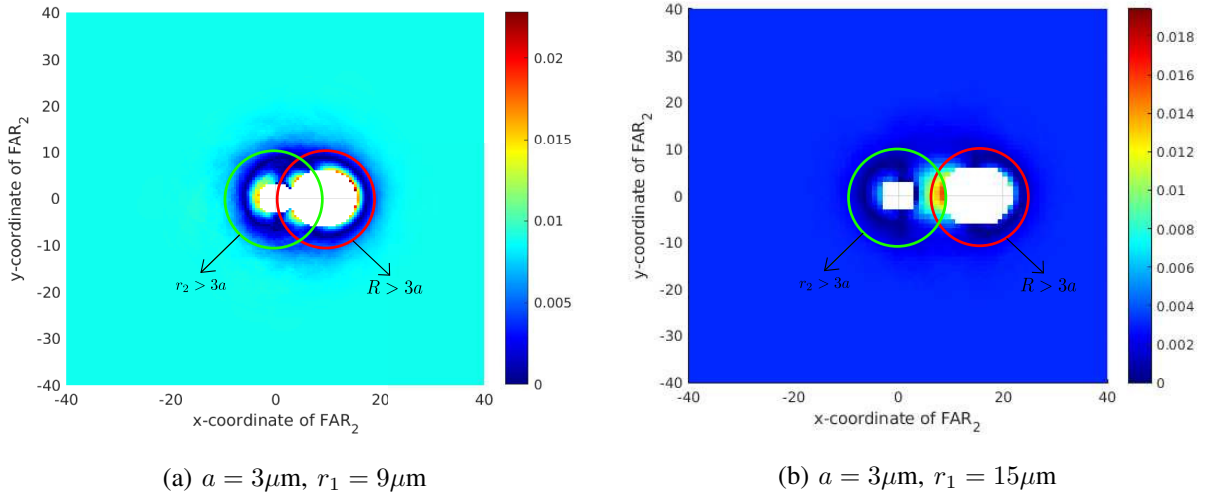
APPENDIX F
GOODNESS OF APPROXIMATION

(a) $a = 3\mu$m, $r_1 = 9\mu$m

(b) $a = 3\mu$m, $r_1 = 15\mu$m

Fig. 5: Approximation error in the hitting probability of IM on FAR_1 in the presence of FAR_2. The error value at a location (x, y) denotes the AE when FAR_2 is located at the location (x, y). Here FAR_1 is at a fixed position $\boldsymbol{x}_1 = [r_1 \ 0 \ 0]$ and FAR_2 is shifted in the X-Y plane.

To understand how accurate the approximation of IM's hitting point at FAR_j by the point E_j in Appendix A is, we perform extensive simulations by varying locations of FAR_1 and FAR_2.

---

[1]The fitting coefficients for positive and negative argument are optimized to minimize the sum of square errors.

Fig. 5 shows the the absolute error (AE) in hitting probability of IM on FAR_1 in the presence of FAR_2, defined as

$$AE = |\text{Analytical value} - \text{Simulation value}|.$$

The error value at a location (x, y) denotes the AE when the FAR_2 is located at the location (x, y) while the location of FAR_1 is fixed at $[r_1, 0, 0]$. From Fig 5, we can see that AE is small at most places where there is no overlap between the FARs (denoted by the white color). In particular, the AE is negligible when $r_2 > 3a$ and $R > 3a$ (denoted by region outside the green and red circles respectively) for $r_1 > 3a$.

REFERENCES

[1] I. F. Akyildiz, M. Pierobon, S. Balasubramaniam, and Y. Koucheryavy, "The internet of bio-nano things," *IEEE Commun. Mag.*, vol. 53, no. 3, pp. 32–40, Mar. 2015.

[2] V. Jamali, A. Ahmadzadeh, W. Wicke, A. Noel, and R. Schober, "Channel modeling for diffusive molecular communicationA tutorial review," *Proc. IEEE*, vol. 107, no. 7, pp. 1256–1301, July 2019.

[3] J. W. Kwack, H. B. Yilmaz, N. Farsad, C.-B. Chae, and A. Goldsmith, "Two way molecular communications," in *Proc. NANOCOM, ACM Press*, Sep. 2018, pp. 1–5.

[4] Y. Lu, M. D. Higgins, A. Noel, M. S. Leeson, and Y. Chen, "The effect of two receivers on broadcast molecular communication systems," *IEEE Trans. Nanobiosci.*, vol. 15, no. 8, pp. 891–900, Dec. 2016.

[5] X. Bao, J. Lin, and W. Zhang, "Channel modeling of molecular communication via diffusion with multiple absorbing receivers," *IEEE Wirel. Commun. Lett.*, vol. 8, no. 3, pp. 809–812, June 2019.

[6] B.-H. Koo, C. Lee, H. B. Yilmaz, N. Farsad, A. Eckford, and C.-B. Chae, "Molecular MIMO: From theory to prototype," *IEEE J. Sel. Areas Commun.*, vol. 34, no. 3, pp. 600–614, Mar. 2016.

[7] A. Berezhkovskii and Y. Makhnovskii, "Mutual influence of traps on the death of a Brownian particle," *Chem. Phys. Lett.*, vol. 175, no. 5, pp. 499–504, Dec. 1990.

[8] L.-S. Meng, P.-C. Yeh, K.-C. Chen, and I. F. Akyildiz, "MIMO communications based on molecular diffusion," in *Proc. GLOBECOM*, Dec. 2012, pp. 5380–5385.

[9] V. Jamali, N. Farsad, R. Schober, and A. Goldsmith, "Diffusive molecular communications with reactive molecules: Channel modeling and signal design," *IEEE Trans. Mol. Biol. Multi-Scale Commun.*, vol. 4, no. 3, pp. 171–188, 2018.

[10] L. Meng, P. Yeh, K. Chen, and I. F. Akyildiz, "On receiver design for diffusion-based molecular communication," *IEEE Trans. Signal Process.*, vol. 62, no. 22, pp. 6032–6044, Sep. 2014.

[11] H. B. Yilmaz, A. C. Heren, T. Tugcu, and C.-B. Chae, "Three-dimensional channel characteristics for molecular communications with an absorbing receiver," *IEEE Commun. Lett.*, vol. 18, no. 6, pp. 929–932, June 2014.

[12] N. M. Blachman, "Noise and its effect on communication," *McGraw-Hill*, 1966.

[13] P. Moulin and V. V. Veeravalli, *Statistical Inference for Engineers and Data Scientists*. Cambridge University Press, 2018.

[14] S. Atapattu, C. Tellambura, and H. Jiang, "Analysis of area under the ROC curve of energy detection," *IEEE Trans. Wireless Commun.*, vol. 9, no. 3, pp. 1216–1225, Mar. 2010.

[15] A. M. Berezhkovskii, Y. A. Makhnovskii, and R. A. Suris, "Wiener sausage volume moments," *Journal of Statistical Physics*, vol. 57, no. 1-2, pp. 333–346, Oct. 1989.

[16] M. Lopez-Benitez and F. Casadevall, "Versatile, accurate, and analytically tractable approximation for the Gaussian Q-Function," *IEEE Trans. Commun.*, vol. 59, no. 4, pp. 917–922, Apr 2011.

[17] A. Jeffrey and D. Zwillinger, *Table of integrals, series, and products.* Elsevier, 2007.